Semnan University

Journal of Heat and Mass Transfer Research

Journal homepage: https://jhmtr.semnan.ac.ir

ISSN: 2383-3068

Research Article

Influence of Coil Geometry on Magnetic Nanoparticle Hyperthermia in the Treatment of Peritoneal Metastasis

Mohadese Ranjbaran [a], Mohammad Hossein Tavakoli [a*], Zahra Keshtpour Amlashi [b], Safoora Nikzad [c]

[a] *Department of Physics, Faculty of Science, Bu-Ali Sina University, Hamadan, Iran*

[b] *Cancer Research Center, Hamadan University of Medical Sciences, Hamadan, Iran*

[c] *Department of Medical Physics, Faculty of Medicine Isfahan University of Medical Sciences, Isfahan, Iran*

ARTICLE INFO

Article history:

Received: 2025-01-24

Revised: 2025-03-04

Accepted: 2025-04-03

Keywords:

Magnetic hyperthermia;

Magnetic nanoparticles;

Magnetic field;

Peritoneal metastasis;

Coil geometry

ABSTRACT

This study examines the impact of magnetic hyperthermia on treating peritoneal metastasis and analyzes the effect of coil geometry. The aim is to evaluate the efficacy of localized heating in eliminating cancer cells while preserving healthy tissue, with a specific focus on the influence of coil geometry on magnetic nanoparticle hyperthermia for treating peritoneal metastasis. Magnetic nanoparticles concentrate heat within the tumor, minimizing damage to surrounding tissues. Magnetic nanoparticles Fe_3O_4 were used to raise tumor temperatures to 42–46°C under an alternating magnetic field. A numerical simulation based on the finite element method was conducted to assess the effects of coil geometry and tumor location on heat transfer. The magnetic field distribution was calculated using Maxwell's equations, while heat generation by nanoparticles was determined through Rosensweig's theory. The Pennes bio-heat transfer equation was then applied to evaluate temperature distribution in both tumor and healthy tissues. The findings indicate that coil geometry significantly affects the distribution of the magnetic field, heat, and temperature. Cylindrical, flat, conical, and inverted conical coils generate the lowest overall heat while ensuring even distribution, leading to minimal temperature variations across the tumor. Therefore, these coils produce a more uniform temperature distribution within gastric tumors and peritoneal metastases. Additionally, they achieve the therapeutic temperature range required for cancer treatment. The temperature in healthy tissue remains around 37°C, confirming the absence of damage. Therefore, the aforementioned coils are the most suitable for use in magnetic hyperthermia as a treatment for gastric cancer and peritoneal metastasis.

1. Introduction

Cancer remains one of the most significant health challenges in recent years, posing a major global concern. This complex disease occurs when abnormal cells multiply uncontrollably in the body. These cells can invade nearby tissues and spread to other parts of the body through the blood flow or lymphatic system, a process called metastasis. When we say cancer is aggressive, it means that cancer cells have invaded nearby tissues or other organs in the body, leading to the

*** Corresponding author.**

E-mail address: *mht@basu.ac.ir*

Cite this article as:

Ranjbaran, M., Tavakoli, M.H., Keshtpour Amlashi, Z. and Nikzad, S., 2025. Influence of Coil Geometry on Magnetic Nanoparticle Hyperthermia in the Treatment of Peritoneal Metastasis. *Journal of Heat and Mass Transfer Research*, 12(2), pp. 413-427.

https://doi.org/10.22075/JHMTR.2025.36686.1677

formation of cancer metastasis [1–3]. Usually, peritoneal metastasis originates in another organ and then moves to the peritoneal cavity. Peritoneal cancer may originate from cancers of the gastric, intestine, colon, uterus, ovaries, and esophagus [4, 5]. Common cancer treatments such as chemotherapy, radiotherapy, and surgery are often used in combination to improve patient outcomes. However, a major challenge with these conventional methods is their inability to selectively target cancer cells without harming healthy tissues. The ideal cancer treatment would be one that effectively destroys cancer cells while minimizing damage to normal tissues. One promising advancement in non-invasive cancer treatment is hyperthermia, a technique that has recently gained acceptance and approval. This method involves controlled heating of tumor tissues to temperatures between 42–46°C, leading to the destruction of cancer cells. Hyperthermia is now being integrated with conventional treatments and has demonstrated a wide range of applications in medical science [6, 7]. There are several methods to induce hyperthermia. One approach involves the use of magnetic nanoparticles (MNPs) in combination with an alternating magnetic field (AMF). In this approach, MNPs act as localized heat sources, increasing the temperature of the tumor. Thermal analysis and precise temperature distribution within the tumor and surrounding healthy tissue are critical factors for the effectiveness of this treatment. Several parameters influence this process, including the frequency, intensity, and distribution of the magnetic field; the properties of MNPs; tumor location; and treatment duration [8–11]. While numerous studies have investigated the use of MNP-based hyperthermia for treating tumors in various parts of the body [12–16], research on its application for peritoneal metastases remains limited due to various challenges and obstacles. Addressing these challenges is crucial for advancing treatment options for patients with peritoneal metastases and improving their prognosis.

Matsumi et al. studied the treatment of peritoneal metastasis that had spread from gastric cancer (peritoneal metastasis of gastric cancer) experimentally and in the lab. The study used a mouse model with peritoneal metastasis cancer. For treatment, a hyperthermia method was used with superparamagnetic iron oxide (Fe3O4) nanoparticles (SPIONs). Finally, they found that magnetic hyperthermia therapy (MHT) is a more effective treatment for peritoneal metastases than other treatment methods. Based on this study, MHT could be used as a new treatment option for peritoneal metastasis [17]. In MHT, an induction coil is required to generate an AMF. Therefore, coil geometry directly influences the intensity and distribution of the magnetic field, heat generation, and temperature distribution in the body [18, 19]. Fig. 1 shows the types of coils used in this study [20, 21].

Rouni et al. have investigated the safety of magnetic hyperthermia systems based on nanoparticles, which use controlled heat to destroy cancer cells in cancer treatment. This research focuses on evaluating the safety of a system that utilizes an AMF and MNPs to generate heat. Practical experiments and empirical data have been used to examine the impact of this system on body temperature [22].

Chia et al. [23] have investigated the effects of hyperthermia and its combination with intraperitoneal drug delivery in the treatment of peritoneal metastases. Initially, the immune status of the healthy peritoneal cavity and the immune structure of peritoneal metastases were examined. Then, the positive and negative effects of hyperthermia and its heat shock response on the tumor immune microenvironment were analyzed. Additionally, the impact of hyperthermia on the biomechanical properties of tumor tissue and its implications for immune cell infiltration were studied.

In addition to SPIONs, several other materials have also been used in hyperthermia treatments. These include various types of MNPs, such as cobalt, nickel, and core-shell nanoparticles. Each of these materials possesses unique properties that make them suitable for inducing localized heat when exposed to AMF. The choice of material can influence factors such as heat generation efficiency, biocompatibility, and magnetic response, which are critical for optimizing the treatment's effectiveness and minimizing adverse effects [24-26]. In this study, we used SPIONs because they are more effective in treating peritoneal metastasis. According to Matsumi et al.'s experimental findings, these nanoparticles exhibit superior performance in generating localized heat when exposed to AMF, making them particularly suitable for targeting metastatic tumors in sensitive areas like the peritoneum. Their ability to selectively heat tumor cells while minimizing damage to surrounding healthy tissue enhances the overall treatment effectiveness [17]. SPIONs to improve thermal and magnetic stability and enhance heating efficiency in hyperthermia treatment. These nanoparticles offer greater safety, reducing the risk of side effects such as clot formation or accumulation in non-target tissues. Moreover, they produce effective heat when exposed to an AMF, making them ideal for cancer cell destruction at controlled temperatures. Their uniform dispersion in biological environments

also leads to better thermal distribution and improved therapeutic efficiency. These characteristics make SPIONs a promising and effective choice for magnetic hyperthermia applications [27].

Recent research in hyperthermia has examined the effects of different nanoparticle shapes [28] and the combination of various heating methods [29]. These studies highlight the importance of optimizing coil design and geometry in cancer treatment, which is investigated in this study.

This study models MHT for treating gastric cancer metastasized to the peritoneum, focusing on the effects of tumor location and coil geometry on achieving uniform temperature distribution. The goal is to optimize coil design for enhanced treatment efficiency using MNPs, ensuring effective cancer cell destruction while minimizing damage to healthy tissue and side effects for patients resistant to existing therapies.

The novelty of this study lies in the optimized design of induction coils to enhance the magnetic field distribution, thereby improving the overall efficacy of MHT. By employing advanced numerical modeling, this research precisely simulates magnetic field interactions with nanoparticles within biological tissues, enabling more accurate predictions of treatment outcomes. Modifications in coil geometry can mitigate treatment-related side effects while enhancing thermal targeting precision. This innovation plays a crucial role in minimizing collateral damage to healthy tissues through refined coil design. Furthermore, this study explores the application of MHT for peritoneal metastases, demonstrating its therapeutic potential in patients resistant to conventional treatments.

The findings of this research hold significant clinical implications, particularly in enhancing the precision and effectiveness of MHT. By designing coil geometries to optimize targeted heat delivery to tumors while minimizing excess heat in non-targeted areas, treatment side effects can be significantly reduced, and treatment accuracy can be improved. Beyond its application in treatment planning for patients with peritoneal metastases, this research provides a framework for designing similar therapies for other cancers, particularly those involving deep-seated or abdominal tumors.

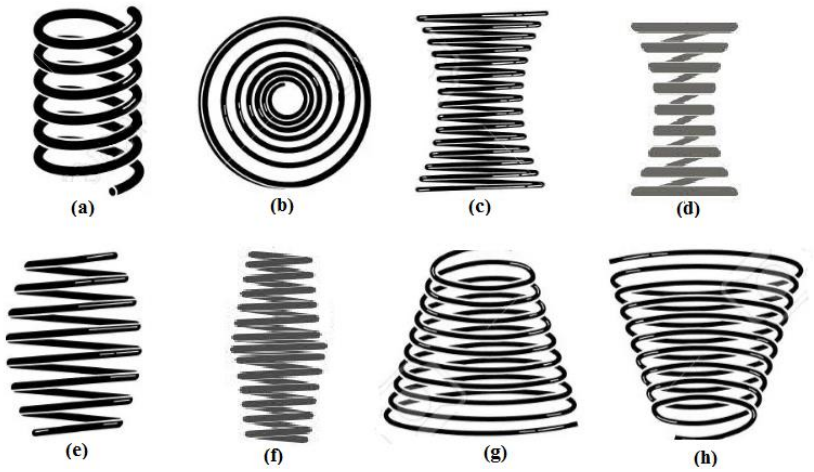

Fig. 1. Types of coils: (a) Cylindrical; (b) Flat; (c) Hourglass; (d) Sharp hourglass; (e) Bbarrel; (f) Sharp barrel; (g) Conical; and (h) Inverted conical [20, 21]

2. Mathematical Model

Fig. 2 is an image of the geometry of the model. As can be seen, the model that was studied is a two-dimensional (2D) model that includes an induction coil, abdominal tissue, and a spherical tumor in the gastric tissue that eventually metastasizes into the peritoneum. Therefore, AMF is applied to the target tissue (the tumor), and the MNPs in the tumor act as a source of heat generation.

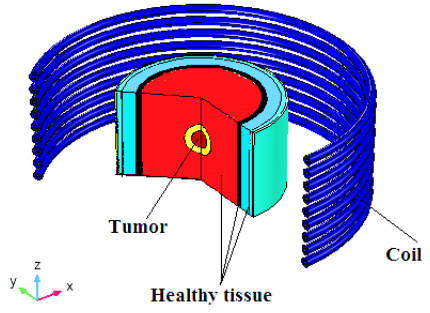

Fig. 2. View of the geometrical model used for MHT

2.1. Model Assumptions

1. The system is linear, isotropic, and stationary.
2. All materials are non-magnetic and have no net electric charge except MNPs inside the tumor.
3. The displacement current density is neglected, and the electric current distribution inside the coil is assumed to be uniform.
4. The system has rotational symmetry around the z-axis.
5. The distribution of MNPs in the tumor is uniform.

2.2. Basic Equations

- **Induction Heating**

In the process of induction heating, the alternating current in the coil generates time-dependent electromagnetic fields in the space around the coil. When a workpiece or electrically conductive object is placed in these fields, eddy currents are generated, and the Joule effect (RI^2) causes heat to be generated [30].

- **Heat Generated by MNPs**

Heat generation by MNPs is obtained as follows [31]:

$$P = \mu_0 \pi \chi_0 f H^2 \frac{2\pi f \tau_{eff}}{1 + (2\pi f \tau_{eff})^2} \quad (1)$$

where P, μ_0, χ_0, f, and H are the power dissipation of MNPs per unit volume, the permeability of free space, equilibrium susceptibility, the frequency of the applied magnetic field, and the magnetic field intensity, respectively.

The effective relaxation time in (1), τ_{eff}, can be described as follows:

$$\tau_{eff} = \frac{\tau_B \tau_N}{\tau_B + \tau_N} \quad (2)$$

where τ_B is the Brownian relaxation time, τ_N is Néel relaxation time.τ_B is defined as follows:

$$\tau_B = \frac{3\eta V_H}{K_B T} \quad (3)$$

where η, K_B and T are the viscosity of the suspension, the Boltzmann constant, and the absolute temperature of MNPs, respectively.
V_M is the volume of MNPs without including their shell. Because of the MNPs' spherical volume, it is defined as $V_M = \pi D^3/6$.
V_H is the volume of the MNPs with a shell. It is defined as $V_H = \pi(D + 2\delta)^3/6$.
where D and δ are the diameter of MNPs and the thickness, respectively.

The equation for the Néel relaxation time is:

$$\tau_N = \frac{\sqrt{\pi}}{2} \tau_0 \frac{exp(\Gamma)}{\sqrt{\Gamma}} \quad (4)$$

where K_{eff} is the anisotropy constant, τ_0 $(\tau_0 = 10^{-9}s)$ is the attempt time, and $\Gamma = \frac{K_{eff} V_M}{K_B T}$.

The equilibrium susceptibility (χ_0) in the Langevin equation expresses it as follows:

$$\chi_0 = \chi_i \frac{3}{\xi} (coth\, \xi - \frac{1}{\xi}) \quad (5)$$

where $\chi_i$and ξ are the initial susceptibility and the Langevin parameter, respectively.
χ_i described as follows $\chi_i = \mu_0 \phi {M_d}^2 V_M / 3K_B T$ and ξ explained as follows:

$$\xi = \mu_0 M_d H V_M / K_B T \quad (6)$$

where M_d and ϕ are the domain magnetization of suspended MNPs and the volume fraction of MNPs, respectively.

To get the temperature distribution during hyperthermia, using Pennes bio-heat transfer equations for healthy tissue and tumor tissue, the following relationships are used, respectively [32]:

$$\rho_1 c_1 \frac{\partial T}{\partial t} = \nabla.(k \nabla T) + \rho_b c_b \omega_b (T_a - T) + Q_{met} \quad (7)$$

$$\rho_2 c_2 \frac{\partial T}{\partial t} = \nabla.(k \nabla T) + \rho_b c_b \omega_b (T_a - T) + Q_{met} + P \quad (8)$$

where ρ_1,ρ_2,ρ_b, c_1, c_2, c_b, k, T, T_a, ω_b, Q_{met}, and P are the tissue density, the tumor density, the blood density, the specific heat of the tissue, the specific heat of the tumor, the specific heat of blood, the thermal conductivity of the tissue, the tissue temperature, and the arterial blood temperature, the blood perfusion rate, the metabolic heat source, and the power dissipation of MNPs per unit volume in the tumor, respectively.

The considered boundary conditions for Pennes bio-heat transfer equations are as follows:

1. On the upper and lower boundaries of the desired model, the heat flux is zero ($\frac{\partial T}{\partial n} = 0$).
2. The temperature on the body surface is considered to be 37 °C.

2.3. Solving the Equations

The finite element method has been used to solve the equations presented in this study. An irregular triangle mesh type is used to do calculations.

Fig. 3 shows a view of the mesh of the studied system. The simulation is based on human dimensions. In the studied model, after injecting SPION into the tumor and achieving a uniform distribution, the target tissue is placed in an AMF by different coils.

These coils consist of 9 rings with a circular surface and a thickness of 0.5 cm made of copper, which are designed with different geometries, including cylindrical, flat, hourglass, sharp hourglass, barrel, sharp barrel, conical, and inverted conical (Fig. 4). For peritoneal metastasis and stomach cancer, MHT sessions usually last between 30 to 60 minutes; however, in this article, the treatment time is a fixed constant. This duration is based on the thermal dose required to destroy cancer cells (usually in the temperature range of 41-46°C) and the tolerance of healthy tissues. However, the exact treatment duration may vary depending on the specific protocols of treatment centers and the equipment used [33, 34].

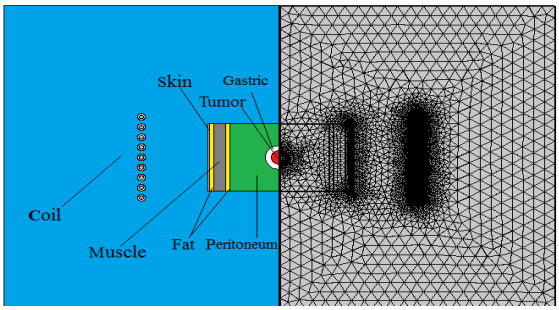

Fig. 3. Computational space (left-hand side) and its mesh for the computation (right-hand side)

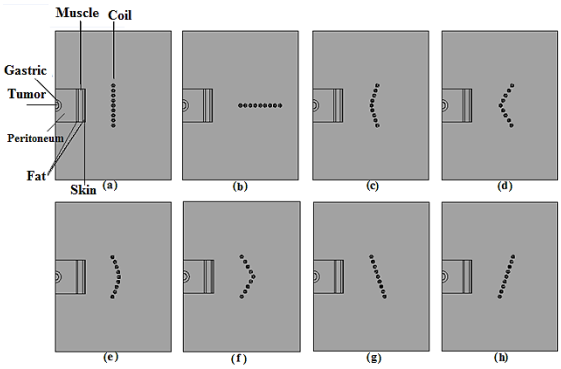

Fig 4. Different coil geometries: (a) Cylindrical; (b) Flat; (c) Hourglass; (d) Sharp hourglass; (e) Barrel, (f) Sharp barrel; (g) Conical; (h) Inverted conical.

In this study, the geometry dimensions of the model, the thermal characteristics of healthy and tumor tissue used to solve the bio-heat transfer equation, and magnetic and MNPs characteristics are presented in Table 1, Table 2, and Table 3, respectively.

Table 1. Geometry dimensions of the model

Properties (characteristic)	Value (cm)	Properties (characteristic)	Value (cm)
Gastric radius	3.5	Inner radius of hourglass and sharp hourglass coils (at narrowest part)	2
Peritoneal cavity radius	13	Outer radius of barrel and sharp barrel coils (at widest part)	5
Muscles	3	Inner radius of barrel and sharp barrel coils (at narrowest part)	2
Extraperitoneal fat and subcutaneous fat	1	Outer radius of conical coil (at widest part)	5
Skin	0.4	Inner radius of conical coil (at narrowest part)	2
Outer radius of cylindrical coil	5	Outer radius of inverted conical coil (at widest part)	5
Inner radius of cylindrical coil	2	Outer radius of inverted conical coil (at narrowest part)	2
Width of flat coil	5	Pitch of all coils	1
Thickness of flat coil	2	Coil length	20
Outer radius of hourglass and sharp hourglass coils (at widest part)	5		

Table 2. The thermal characteristics of healthy and tumor tissue used to solve the bio-heat transfer equation [35-38]

Parameters	Blood	Skin	Fat	Muscle	Peritoneum	Gastric	Tumor
Specific heat (J/kgK)	3770	3391	2348	3421	3600	3690	3690
Density (kg/m3)	1060	1109	911	1090	1055	1088	1088
Thermal Conductivity (W/mK)	0.52	0.37	0.21	0.49	0.51	0.53	0.53
Blood perfusion rate (1/S)	-	0.05	0	0.00187	0.018	0.00187	0.002
Metabolic heat (W/m3)	-	368.1	368.3	1190	5000	1190	31872

Table 3. Magnetic and MNP (Fe_3O_4) properties used in the simulation [10, 31-39]

Parameters	Values	Unit
M_d	446	kA/m
K_{eff}	9	kJ/m^3
τ_0	10^{-9}	s
δ	1	nm
K_B	1.38×10^{-23}	J/K
D	19	nm
f	100	kHz
φ	0/071	-
I	100	A

3. Results and Discussion

In this part, the results of magnetic field intensity and distribution, induction heating, heat generated by MNPs, and temperature distribution for the treatment of a human model of peritoneal metastasis cancer are presented. First, the magnetic field distribution and induction heating with different coil geometries are shown. Then, heat and temperature distribution in tumor and healthy tissue are discussed. Finally, the geometry change of the coil and its influence on the heat and temperature distribution of the target tumor have been evaluated. For calculations, two states are considered for the location of the tumor: (a) the state where the tumor is located in the gastric, and (b) the state where peritoneal metastasis has occurred.

For all considered coils, although the structure of the AMF inside the coils is different, the structure of the AMF is almost the same outside the coils. Because the studied parts (healthy tissue and tumor) are located in the inner space of the coils, we focus our attention only on the structure of the AMF in the inner space of the coils. The target tissue (workpiece) tries to expel the components of the AMF from within itself, thus making them more intense in the space between the tissue and the coil than in other places. In all coils, the magnetic flux is more intense in the space between the ring and the tissue than in other places. Also, due to the skin effect, the magnetic field intensity on the surface of the rings is always more intense than in other areas, and this intensity decreases as we move away from the surface of the rings [38]. As can be seen in Fig. 5, in the state where the tumor is in the gastric, the magnetic field intensity distribution by cylindrical, flat, hourglass, sharp hourglass, barrel, and sharp barrel coils, in the center of the tumor, and finally in the right and left sides of the tumor, has its maximum value. In the conical coil, the magnetic field intensity distribution decreases from top to bottom, and the maximum value of the magnetic field is at the top of the tumor. In the inverted conical coil, the magnetic field intensity distribution increases from top to bottom, and the maximum value of the magnetic field is at the bottom of the tumor. In Fig. 6, in the state where the tumor has metastasized in the peritoneum, in all the coils, the distribution of magnetic field intensity within the cancer tissue decreases from top to bottom, and the maximum value of the magnetic field is above the tumor. The percentage changes in the magnetic field intensity by different coils in the tumor are shown in Table 4. The results indicate that as the percentage of magnetic field variations increases, the magnetic field distribution becomes increasingly non-uniform. This study aims to achieve a uniform magnetic field distribution; therefore, reducing the percentage of field variations would positively impact our performance.

3.1. Magnetic Field

In Figs. 5 and 6, the distribution of the magnetic field intensity in the tumor is shown for two locations of the tumor (gastric cancer and peritoneal metastasis), respectively.

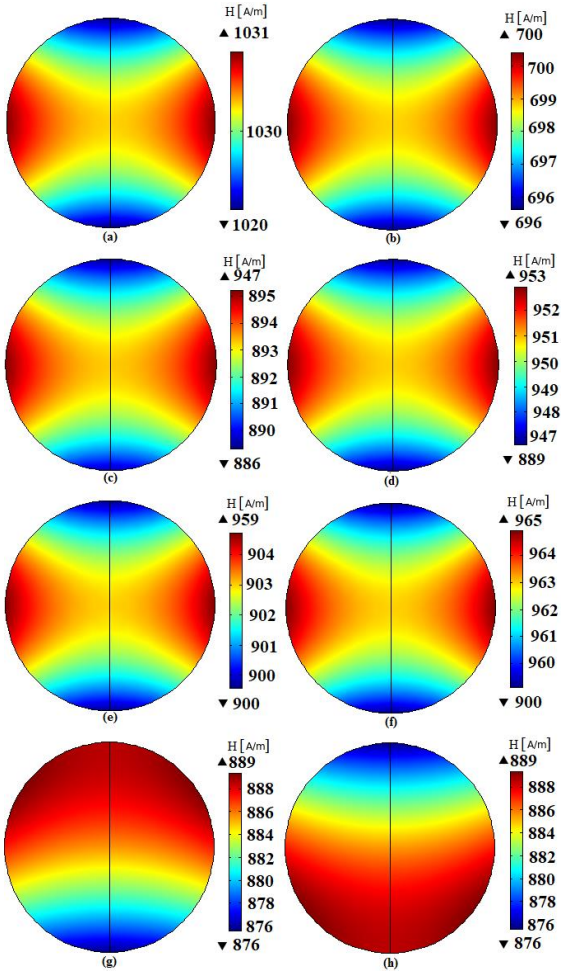

Fig. 5. Magnetic field distribution in the tumor (gastric cancer) by the coil: (a) Cylindrical; (b) Flat; (c) Hourglass; (d) Sharp hourglass, (e) Barrel; (f) Sharp barrel; (g) Conical; (h) Inverted conical

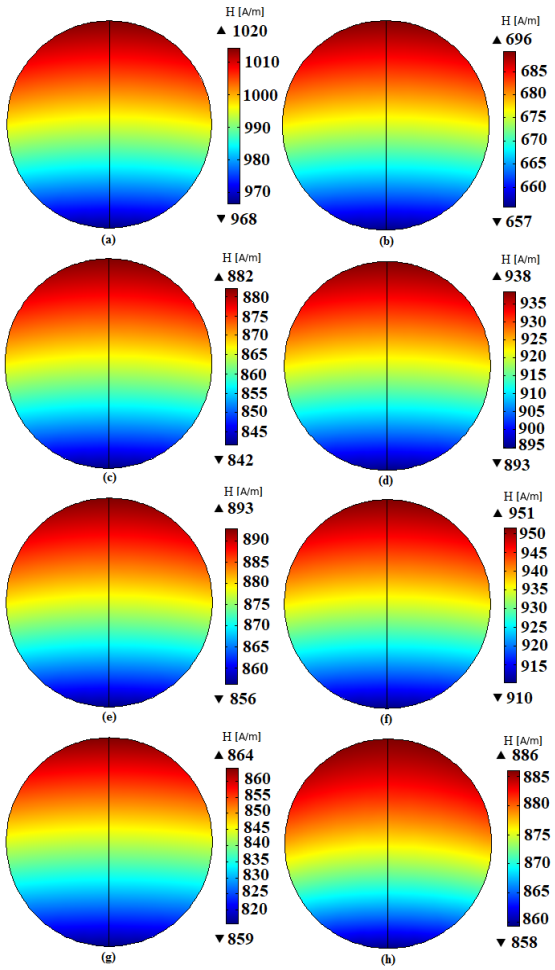

Fig. 6. Magnetic field distribution in the tumor (peritoneal metastasis) by the coil: (a) Cylindrical; (b) Flat; (c) Hourglass; (d) Sharp hourglass; (e) barrel; (f) sharp barrel; (g) conical; (h) Inverted conical

Table 4. Percentage changes in the magnetic field intensity.

Type of coil	Percentage changes in the magnetic field in gastric cancer	Percentage changes in the magnetic field in peritoneal metastasis
Cylindrical	0.9	0.9
Flat	0.5	1
Hourglass	6.7	4.4
Sharp hourglass	5.4	4.5
Barrel	6.7	4.3
Sharp barrrel	5.6	4.1
Conical	1.4	0.5
Inverted conical	1.4	0.2

3.2. Induction Heating

In this part, the heat generated by the eddy currents (induction heating) in the tumor has been calculated for all considered coils. Fig. 7 shows the distribution induction heating in the peritoneal metastasis.

According to these figures, in the tumor, the maximum amount of induction heating is located on its outer surface. Induction heating changes from the surface to the center of the tumor are caused by the skin effect (a phenomenon that causes a non-uniform distribution of alternating current in the cross-sectional area of the conductor) [40]. As can be seen, due to the skin effect, the maximum amount of heat is on the outer surface of the tumor, and as we move from this level toward the center, the amount of heat decreases. Also, the maximum heat generated on the tumor surface due to the proximity effect (a phenomenon that affects the heat distribution in a conductor when it is in the vicinity of another conductor) leads to hot points on the surface of the tumor.

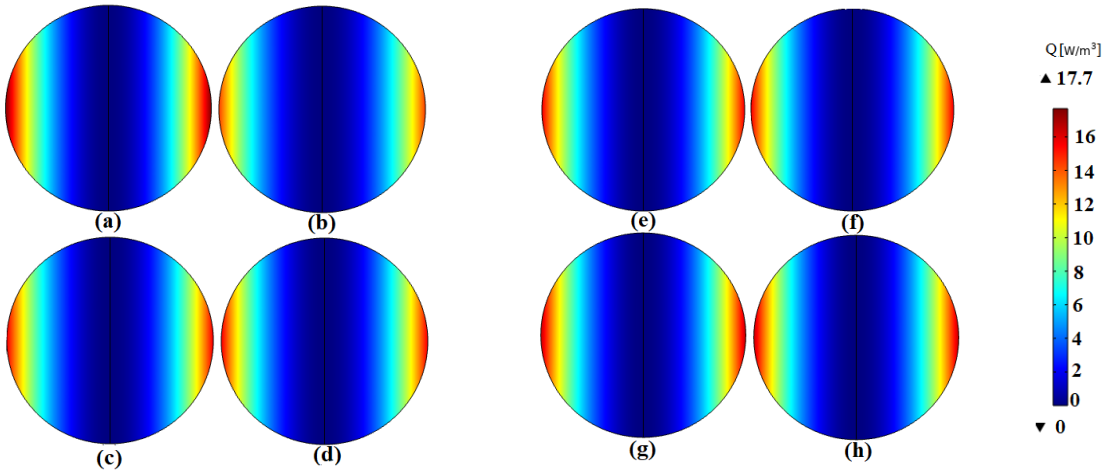

Fig. 7. The distribution of heat generated by eddy currents in the peritoneal metastasis for the coil: (a) Cylindrical; (b) Flat; (c) hourglass; (d) Sharp hourglass; (e) Barrel; (f) Sharp barrel; (g) Conical, and (h) Inverted conical

3.3. Distribution of Heat Generated by MNPs in Tumors

In this part, we assume that MNPs are distributed only in the tumor, so the heat generated by MNPs is only inside the tumor, and this makes the tissue around the tumor remain healthy.

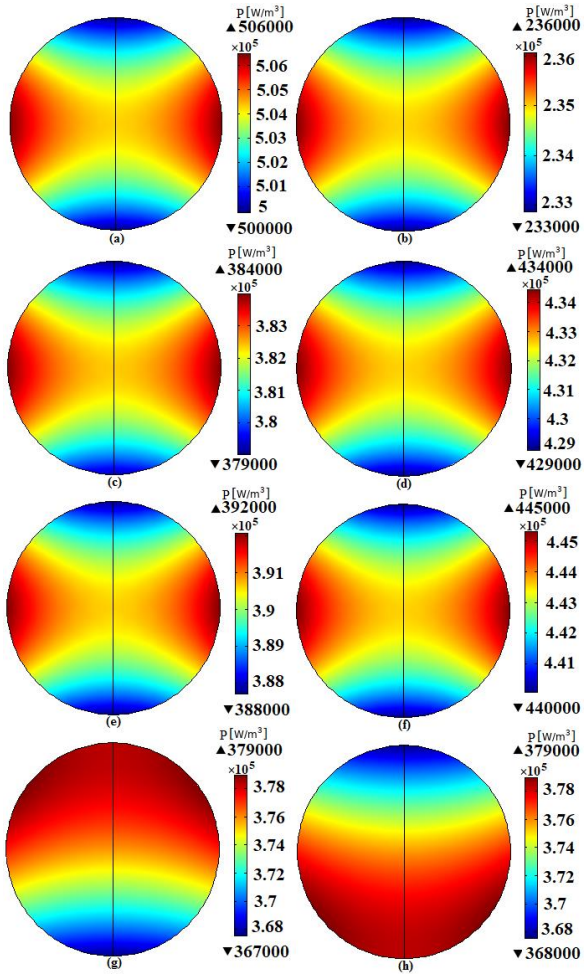

Fig. 8. Heat distribution in the gastric tumor for the coil: (a) Cylindrical; (b) Flat; (c) Hourglass; (d) Sharp hourglass, (e) Barrel; (f) Sharp barrel; (g) Conical; (h) Inverted conical.

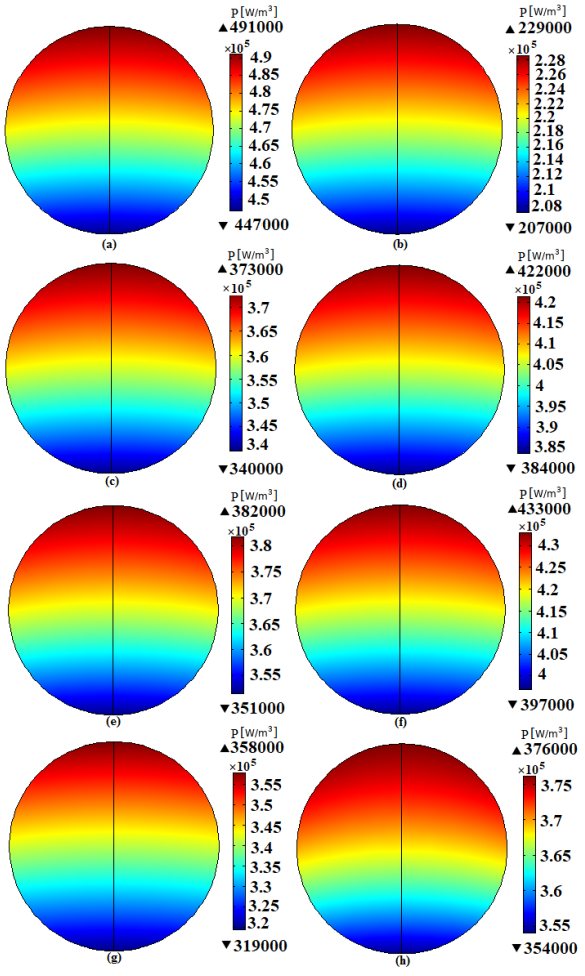

Fig. 9. Heat distribution in peritoneal metastasis for the coil: (a) Cylindrical; (b) Flat; (c) Hourglass; (d) Sharp hourglass; (e) barrel; (f) sharp barrel; (g) conical; (h) Inverted conical.

Since one of the important factors in heat generation by MNPs is the intensity of the magnetic field, due to the non-uniformity of the magnetic field intensity in different parts of the tumor, the heat distribution is also different (according to equation 2). Considering that in cylindrical, flat, hourglass, sharp hourglass, sharp hourglass, barrel, and sharp barrel coils, the magnetic field intensity in the middle part of the gastric tumor is higher than in the upper and lower parts, so the maximum value of the heat generated in the middle part of the gastric tumor is located. However, in the conical coil, the magnetic field intensity in the upper part of the gastric tumor is higher than in the lower parts, so the maximum value of the heat generated is in the upper part of the gastric tumor. In the inverted conical coil, the magnetic field intensity in the lower part of the gastric tumor is more intense than in the higher parts, so the maximum heat generation is located in the lower part of the gastric tumor. But when the tumor is in the peritoneum, the magnetic field intensity in the upper part of the peritoneal tumor is higher than in its other parts in all the coils, so the maximum heat generation is in the upper part of the peritoneal tumor. From the comparison of the heat generated by MNPs in the tumor (for both gastric and peritoneum) by different coils, it can be seen that the most heat is generated by the hourglass, sharp hourglass, barrel, and sharp barrel coils.

Because in these coils, the magnetic flux density (magnetic field distribution) generated due to these coils is higher than in other coils (the percentage changes in magnetic field intensity in these coils are higher than in other coils). In these coils, the rings are the closest distance from the tumor compared to other models, so the magnetic field intensity in the tumor is higher than in other coils, and as a result, more heat is generated in the tumor than in other models. Since induction heating has a very small value compared to heat generation by MNPs, the heat generated by MNPs in the tumor can be considered total heat (Table 5).

Table 5. Total heat in gastric cancer and peritoneal metastasis

Type of coil	The heat of MNPs in gastric cancer (W)	Induction heating gastric cancer (W)	The heat of MNPs in peritoneal metastasis (W)	Induction heating for peritoneal metastasis (W)
Cylindrical	11.9	1.7×10^{-4}	11.4	1.7×10^{-4}
Flat	7.9	1.2×10^{-4}	7.1	1.1×10^{-4}
Hourglass	14.8	2.4×10^{-4}	14.2	2.2×10^{-4}
Sharp hourglass	14.5	2.3×10^{-4}	14.6	2.3×10^{-4}
Barrel	13.9	2.2×10^{-4}	13.6	2.1×10^{-4}
Sharp barrrel	13.8	2.3×10^{-4}	13.7	2.2×10^{-4}
Conical	12.6	1.8×10^{-4}	12.2	1.6×10^{-4}
Inverted conical	12.6	1.8×10^{-4}	12.2	1.6×10^{-4}

3.4. Temperature Distribution in Tumor and Tissue

As mentioned earlier, to obtain the temperature distribution of the tumor, the results of the power dissipation of MNPs per unit volume in the tumor (heat generation by MNPs) by different coils have been entered as input in the Pennes bio-heat transfer equations (Equations 7 and 8). Figs. 10 and 11 show the temperature distribution in the gastric tumor and peritoneal metastasis, respectively. Figures 12 and 13 show the temperature distribution in the gastric tumor and tissue, as well as in peritoneal and tissue metastasis, respectively.

In all models, the maximum temperature generated in the tumor is located on the axis of symmetry ($r = 0$) and its central part. As we move away from the central area of the tumor, due to the transfer of heat to the healthy tissue and other parts, the temperature of the tumor decreases, so that the lowest temperature generated in all the coils is on the surface of the tumor and the boundary of its separation from the healthy tissue (Figs. 10 and 11). The results show that the temperature generated in the cylindrical, flat, conical, and inverted conical coils has reached the desired therapeutic temperature range of 41–46°C. The minimum temperature difference between the central areas and the surface of the gastric tumor is 4.9°C for the cylindrical coil, 5°C for the conical and inverted conical coils, and 1.5°C for the flat coil. In the peritoneal tumor, the minimum temperature difference between the central areas and the surface of the tumor is 4.7°C for cylindrical, conical, and inverted conical coils and 4.8°C for flat coils. This indicates a more uniform

temperature distribution in the tumor (gastric and peritoneal metastasis) caused by these coils. However, in other coil geometries, the tumor temperature does not reach this treatment temperature range. In these cases, if the lowest temperature is raised to 41°C (sufficient to begin tumor destruction), the highest temperature exceeds 47°C, causing damage to surrounding tissues. Conversely, if the highest temperature is limited to 47°C, the lowest temperature does not reach 41°C, leaving parts of the tumor untreated. These result in non-uniform temperature distribution, reducing treatment effectiveness and increasing risks to healthy tissues.

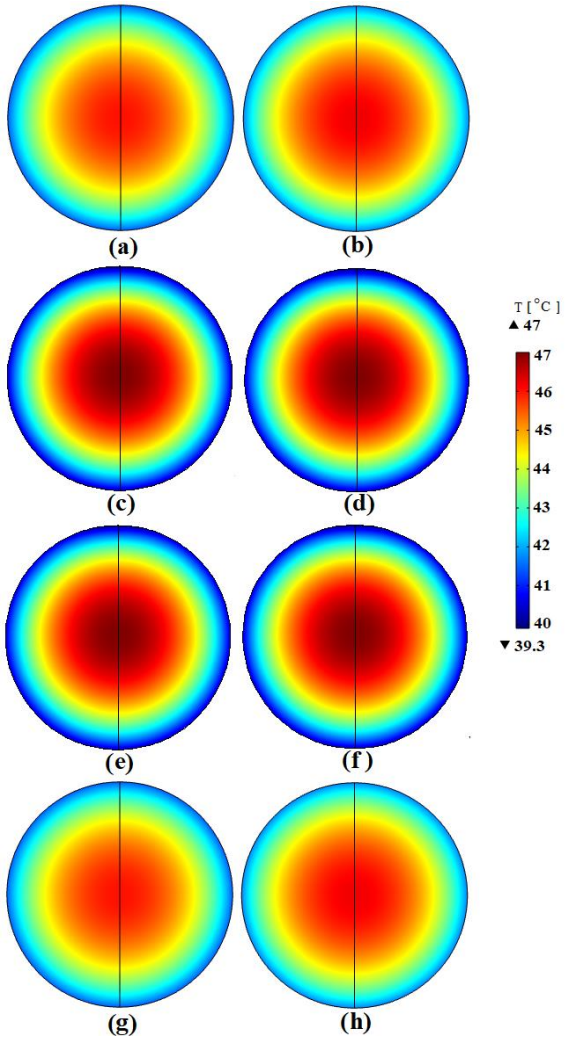

Fig. 10. Temperature distribution in the gastric tumor for the coil: (a) Cylindrical; (b) Flat; (c) Hourglass; (d) Sharp hourglass, (e) Barrel; (f) Sharp barrel; (g) Conical; (h) Inverted conical.

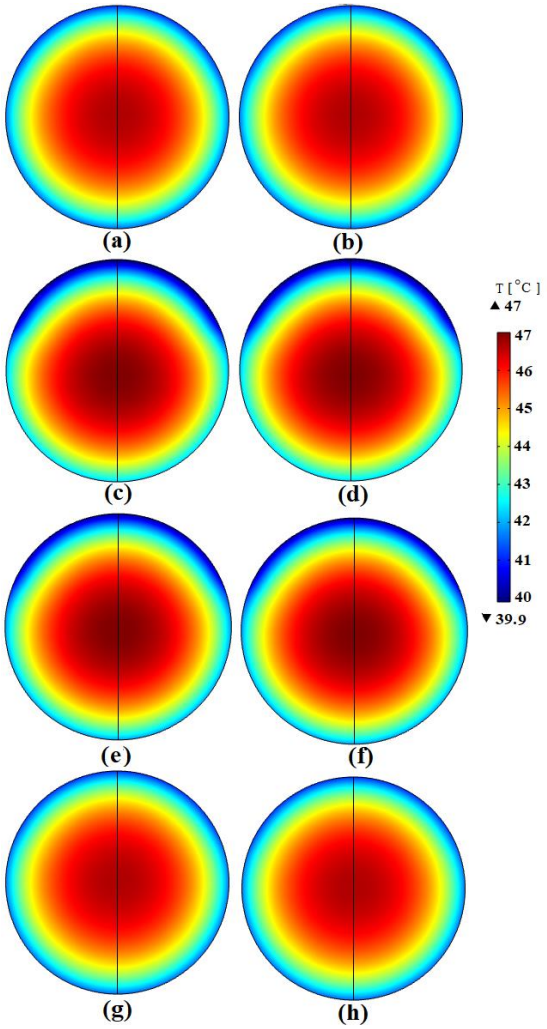

Fig. 11. Temperature distribution in peritoneal metastasis for the coil: (a) Cylindrical; (b) Flat; (c) Hourglass; (d) Sharp hourglass; (e) barrel; (f) sharp barrel; (g) conical; (h) Inverted conical.

Studies show that when the temperature exceeds 45°C, tissue damage occurs and cell death happens [41]. As observed, the temperature at the center of the tumor is the highest and decreases as one moves away from the center of the tumor (due to heat transfer from the surrounding tissue). The temperature in areas far from the tumor is 37°C. The temperature in the tissues surrounding the tumor increases slightly, but this increase is not enough to damage healthy tissue (less than 45°C). This is a desirable feature of hyperthermia with magnetic nanoparticles, which localizes the heat and prevents damage to the surrounding tissue. As can be seen, the temperature value in healthy tissue is about 37°C, which indicates that the healthy tissue is not damaged (Figs. 12 and 13).

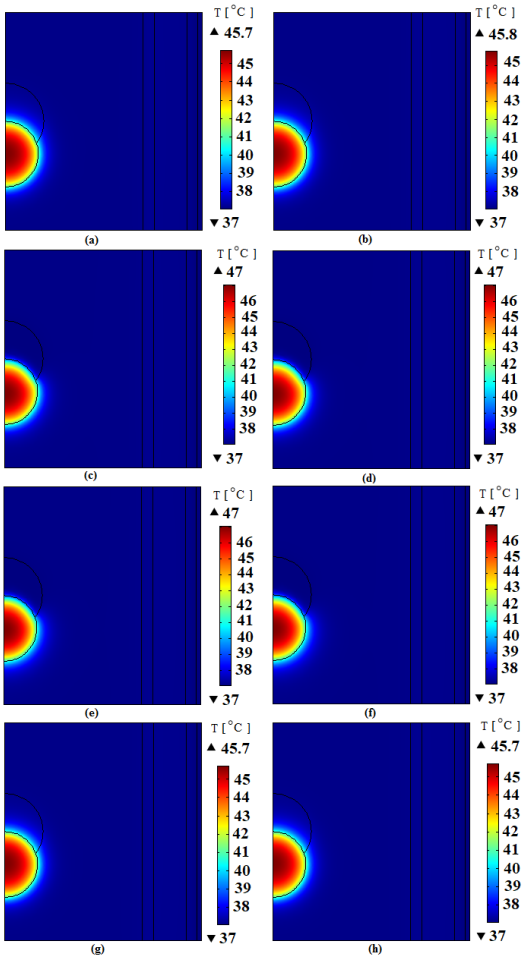

Fig. 12. Temperature distribution in peritoneal metastasis and healthy tissue for the coil: (a) Cylindrical; (b) Flat; (c) Hourglass; (d) Sharp hourglass, (e) Barrel; (f) Sharp barrel; (g) Conical; (h) Inverted conical

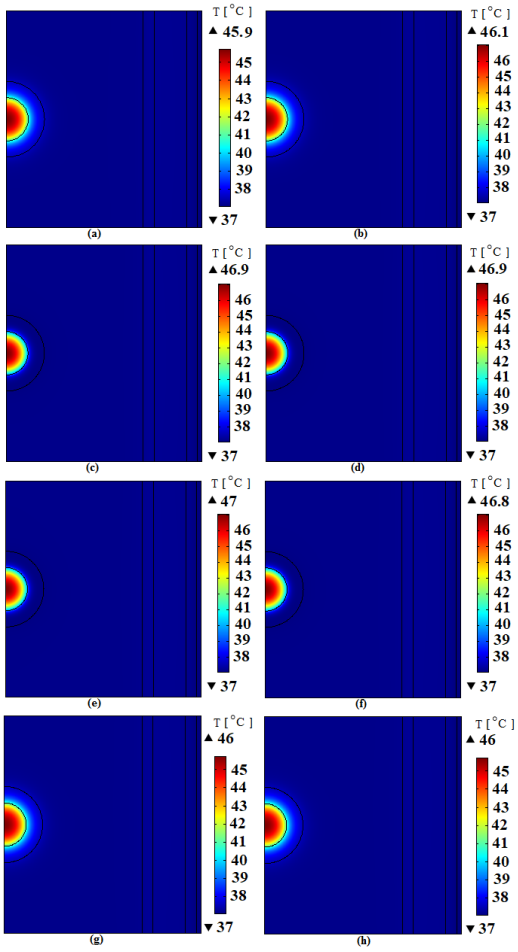

Fig. 13. Temperature distribution in gastric tumor and healthy tissue for the coil: (a) Cylindrical; (b) Flat; (c) Hourglass; (d) Sharp hourglass; (e) barrel; (f) sharp barrel; (g) conical; (h) Inverted conical

For a better evaluation of the temperature distribution and a better comparison of the models, the curve of the tumor temperature distribution on the axis of symmetry for the eight coils used in this research is shown in Fig. 14. As can be seen, the temperature distribution curves of cylindrical, flat, conical, and inverted conical coils were similar. In these models, the temperature generated on the symmetry axis of the tumor is more uniform than in other models, and their diagram has less curvature and more symmetry. But in the hourglass and sharp hourglass, barrel, and sharp barrel models, the changes in the diagram are higher than in other models, and the diagram has more curvature, which indicates a more non-uniform temperature distribution in these curves.

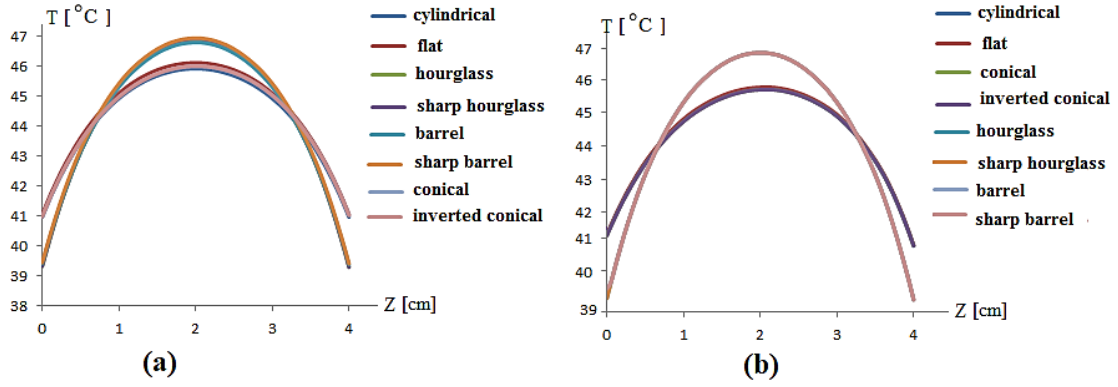

Fig. 14. Temperature distribution in (a) Gastric tumor; (b) Peritoneal metastasis for different coils

4. Discussion and Validation with Experimental Studies

The studies conducted by Matsumi et al. [17], Rouni et al. [22], and Chia et al. [23] all highlight the positive effects of magnetic hyperthermia (MHT) in the treatment of peritoneal metastasis. Their findings demonstrate that the use of superparamagnetic iron oxide nanoparticles (SPIONs) can increase tumor temperature, enhance penetration into cancer cells, and lead to a reduction in tumor size. Moreover, this approach enables localized targeting without inducing systemic toxicity. The present study corroborates these findings through numerical simulations, showing that tumor location and coil geometry significantly impact heat distribution and treatment efficiency. Our results indicate that optimizing these factors can considerably enhance the effectiveness of hyperthermia therapy. In this study, we successfully achieved the therapeutic temperature range of 41 to 45°C, which is sufficient for cancer cell destruction. The study by Rouni et al. focuses on the validation of magnetic hyperthermia systems, employing a combination of experimental measurements and numerical modeling to analyze the distribution of the alternating magnetic field (AMF) and temperature rise in the torso region of patients. Their results, which show a strong correlation between simulated and clinical data, further validate the accuracy of our computational models. These findings play a crucial role in improving the design of magnetic hyperthermia systems, enhancing treatment efficacy, and ensuring patient safety. Additionally, the study by Chia et al. examines the effects of hyperthermia on the tumor immune microenvironment and the biomechanical properties of tumor tissue. Their findings suggest that elevated temperatures can enhance immune cell infiltration into tumors, which may improve treatment outcomes. Our study also confirms this effect by comparing clinical data with simulation results. Previous studies, along with our findings, indicate that magnetic nanoparticle hyperthermia is an effective and safe treatment approach for peritoneal metastasis. However, further research is required to optimize treatment parameters, assess its impact on different cancer types, and explore its integration with combination therapies such as chemotherapy and immunotherapy. Future studies should focus on advanced numerical modeling, extensive clinical measurements, and in-depth biological mechanism investigations to further refine and enhance this therapeutic approach.

5. Conclusions

In this paper, the effect of different coil geometries (cylindrical, flat, hourglass, sharp hourglass, barrel, sharp barrel, conical, and inverted conical) on the distribution of magnetic field intensity, generated heat, and temperature distribution in gastric cancer and peritoneal metastasis during the MHT was investigated. The system was solved using the two-dimensional finite element method. The results obtained from the numerical calculations of MHT showed that:

1. The magnetic field generated by different coil geometries is non-uniform in different areas of the tumor. The highest magnetic field intensity is generated by hourglass, sharp hourglass, barrel, and sharp barrel coils. The lowest magnetic field intensity is generated by cylindrical, flat, conical, and inverted conical coils.
2. The heat generated in tumors by cylindrical, flat, conical, and inverted conical coils has a more uniform heat distribution than other coils. The lowest generated heat is related to cylindrical, flat, conical, and inverted conical coils.
3. In all cases, the highest temperature is in the central area of the tumor. Also, the results show that the tumor temperature field for cylindrical, flat, conical, and inverted conical coils had a more uniform temperature distribution than other coils. The temperature difference all over the tumor is less than in other models.
4. It was observed that in hourglass, sharp hourglass, barrel, and sharp barrel coils, the desired temperature for tumor destruction (i.e., 41–46°C) cannot be reached. But in cylindrical, flat, conical, and inverted conical coils, this treatment temperature can be achieved.
5. The temperature value in the healthy tissue was about 37°C, which indicates that the healthy tissue is not damaged. Therefore, it can be concluded that the use of cylindrical, flat, conical, and inverted conical coils in MHT is more suitable for the treatment of gastric cancer and peritoneal metastasis (tumor in both positions) than other geometries.

Nomenclature

P	Power dissipation of MNPs per unit volume
μ_0	Permeability of free space

χ_0	Equilibrium susceptibility
f	Frequency of the applied magnetic field
H	Magnetic field intensity
τ_{eff}	Effective relaxation time
τ_B	Brownian relaxation time
τ_N	Néel relaxation time
η	Viscosity of the suspension
K_B	Boltzmann constant
T	Absolute temperature of MNPs
V_M	Volume of MNPs without including their shell
V_H	Volume of the MNPs with a shell
D	Diameter of MNPs
δ	Thickness of MNPs
K_{eff}	Anisotropy constant
χ_i	Initial susceptibility
ξ	Langevin parameter
M_d	Domain magnetization of suspended MNPs
ϕ	Volume fraction of MNPs
ρ_1	Tissue density
ρ_2	Tumor density
ρ_b	Blood density
c_1	Specific heat of the tissue
c_2	Specific heat of the tumor
c_b	Specific heat of blood
k	Thermal conductivity of the tissue
T	Tissue temperature
T_a	Arterial blood temperature
ω_b	Blood perfusion rate
Q_{met}	Metabolic heat source

Funding Statement

The authors appreciate the Bu-Ali Sina University for financial support through the Grant number 1002763.

Conflicts of Interest

The author declares that there is no conflict of interest regarding the publication of this article.

Authors Contribution Statement

Mohadese Ranjbaran: Formal Analysis; Investigation; Software; Writing – Original Draft.

Mohammad Hossein Tavakoli: Conceptualization; Methodology; Supervision; Review & Editing.

Zahra Keshtpour Amlashi: Data Curation; Review & Editing.

Safoora Nikzad: Data Curation; Review & Editing.

References

[1] Siegel, R. L., Miller, K. D., Wagle, N. S., Jemal, A., 2023. Cancer statistics. *CA: A Cancer Journal for Clinicians*, 73(1), pp. 17–48.

[2] Sudhakar, A., 2009. History of cancer: ancient and modern treatment methods. *Journal of Cancer Science and Therapy*, 1, pp. 1. doi:10.4172/1948-5956.100000e2

[3] Valastyan, S., Weinberg, R.A., 2011. Tumor metastasis: molecular insights and evolving paradigms. *Cell*, 147, pp. 275-292.

[4] Cortés-Guirial, D., Hübner, M., Alyami, M., Bhatt, A., Ceelen, W., Glehen, O., Lordick, F., Ramsay, R., Sgarbura, O., Speeten, K.V., Turaga, K.K., Chand, M., 2021. Primary and metastatic peritoneal surface malignancies. *Nature Reviews Disease Primers*, 7, p. 91.

[5] Coccolini, F., Gheza, F., Lotti, M., Virzi, S., Iusco, D., Ghermandi, C., Melotti, R., Baiocchi, G., Giulini, S.M., Ansaloni, L., Catena, F., 2013. Peritoneal carcinomatosis. *World Journal of Gastroenterology*, 19(41), pp. 6979-6994.

[6] Rao, W., Deng, Z. S., 2010. A review of hyperthermia combined with radiotherapy/chemotherapy on malignant tumors. *Critical Reviews in Biomedical Engineering*, 38(1), pp. 1-22. doi:10.1615/CritRevBiomedEng.v38. i1.80

[7] Hedayatnasab, Z., Abnisa, F., Wan Daud, W., 2017. Review on magnetic nanoparticles for magnetic nanofluid hyperthermia application. *Materials and Design*, 123, pp. 174-196. doi: 10.1016/j.matdes.2017.03.036

[8] Darvishi, V., Navidbakhsh, M., Amanpour, S., 2022. Heat and mass transfer in the hyperthermia cancer treatment by magnetic nanoparticles. *Heat and Mass Transfer*, 58, pp. 1029–1039. doi: 10.1007/s00231-021-03161-3

[9] Peiravi, M., Eslami, H., Ansari, M., Zare-Zardini, H., 2022. Magnetic hyperthermia: Potentials and limitations. *Journal of the Indian Chemical Society*, 99, pp. 100269. doi: 10.1016/j.jics.2021.100269

[10] Rajan, A., Sahu, N. K., 2020. Review on magnetic nanoparticle-mediated hyperthermia for cancer therapy. *Journal of Nanoparticle Research*, 22, pp. 319. doi:10.1007/s11051-020-05045-9

[11] Avugadda, S. K., Fernandez-Cabada, T., Soni, N., Cassani, M., Mai, B. T., Chantrell, R., Pellegrino, T., 2021. Magnetic nanoparticles and clusters for magnetic hyperthermia: optimizing their heat performance and developing combinatorial therapies to tackle cancer. *Chem. Soc. Rev*. 50, pp. 11614–11667. doi: 10.1039/D1CS00427A

[12] Johannsen, M., Thiesen, B., Wust, P., Jordan, A., 2010. Magnetic nanoparticle hyperthermia for prostate cancer. *International Journal of Hyperthermia*, 26, pp. 790-795. doi: 10.3109/02656731003745740

[13] Golneshan, A.A., Lahonian, M., 2011. Diffusion of magnetic nanoparticles in a multi-site injection process within a biological tissue during magnetic fluid hyperthermia using lattice Boltzmann method. *Mechanics Research Communications*, 38, pp. 425-430. doi: 10.1016/j.mechrescom.2011.05.012

[14] Lahonian, M., Golneshan, A.A., 2011. Numerical study of temperature distribution in a spherical tissue in magnetic fluid hyperthermia using lattice Boltzmann method. *IEEE Transactions on NanoBioscience*, 10, pp. 262-268. doi: 10.1109/TNB.2011.2177100

[15] Adhikary, K., Banerjee, M., 2016. A thermo fluid analysis of the magnetic nanoparticles enhanced heating effects in tissues embedded with large blood vessels during magnetic fluid hyperthermia. *Journal of Nanoparticles*, pp. 6309231. doi: 10.1155/2016/6309231

[16] Liu, W., Chen, X., 2015. Numerical analysis of electromagnetically induced heating and bioheat transfer for magnetic fluid hyperthermia. *IEEE Transactions on Magnetics*, 51, pp. 1-4. doi: 10.1109/TMAG.2014.2358268

[17] Matsumi, Y., Kagawa, T., Yano, S., Tazawa, H., Shigeyasu, K., Takeda, Sh., Ohara, T., Aono, H., Hoffman, R.M., Fujiwara T., Kishimoto, H., 2021. Hyperthermia generated by magnetic nanoparticles for effective treatment of disseminated peritoneal cancer in an orthotopic nude-mouse model. *Cell Cycle*, 20, pp. 1122–1133 doi: 10.1080/15384101.2021.1919441

[18] Shoshiashvili, L., Shamatava, I., Kakulia, D., Shubitidze, F., 2023. Design and Assessment of a novel biconical human-sized alternating magnetic field coil for MNP hyperthermia treatment of deep-seated cancer. *Cancers*, 15, pp. 1672. doi: 10.3390/cancers15061672

[19] Attaluri, A., Jackowski, J., Sharma, A., Kandala, S. K., Nemkov, V., Yakey, Ch., DeWeese, Th.L., Kumar, A., Goldstein, R. C., 2020. Design and construction of a Maxwell-type induction coil for magnetic nanoparticle hyperthermia. *International Journal of Hyperthermia*, 37, pp. 1–14. doi: 10.1080/02656736.2019.1704448

[20] Bobade, R. S., Yadav, Sh. K., 2017. Lateral forces in the helical compression Sspring. *International Journal for Research in Applied Science & Engineering Technology*, 5(4), pp. 98-102.

[21] Misron, N., Ying, L. Q., Firdaus, R. N., Abdullah, N., Mailah N. F., Wakiwaka, H., 2011. Effect of inductive coil Sshape on sensing performance of linear displacement sensor using thin inductive coil and pattern guide. *Sensors*, 11, pp. 10522-10533. doi: 10.3390/s111110522

[22] Rouni, M.A., Shalev, B., Tsanidis, G., Markakis, I., Kraus, S., Rukenstein, P., Suchi, D., Shalev, O., Samaras, T., 2024. A validated methodological approach to prove the safety of clinical electromagnetic induction systems in magnetic hyperthermia. *Cancers*, 16, pp. 621. doi: 10.3390/cancers16030621

[23] Chia, D.K., Demuytere, J., Ernst, S., Salavati, H., Ceelen, W., 2023. Effects of hyperthermia and hyperthermic intraperitoneal chemoperfusion on the peritoneal and tumor immune contexture. *Cancers*, 15, pp. 4314. doi: 10.3390/cancers15174314

[24] Dev, K., Kadian, A., Manikandan, V., Pant, M., Mahapatro, A.K., Annapoorni, S., 2025. Annealing influence on the magnetic and thermal stability of FeNi3 nanoparticles for magnetic hyperthermia applications. *Materials Today Communications*, 43, pp. 111669. doi: 10.1016/j.mtcomm.2025.111669

[25] Singh, A., Kumar, P., Pathak, S., Jain, K., Garg, P., Pant, P., Mahapatro, A.K., Singh, R.K., Rajput, P., Kim, S.K., Maurya, K.K., Pant, R.P.,

2024. Tailored nanoparticles for magnetic hyperthermia: Highly stable aqueous dispersion of Mn-substituted magnetite superparamagnetic nanoparticles by double surfactant coating for improved heating efficiency. *Journal of Alloys and Compounds*, 976, pp. 172999. doi: 10.1016/j.jallcom.2023.172999

[26] Salati, A., Ramazani, A., Kashi, M.A., 2020. Tuning hyperthermia properties of FeNiCo ternary alloy nanoparticles by morphological and magnetic characteristics. *Journal of Magnetism and Magnetic Materials*, 498, pp. 166172. doi: 10.1016/j.jmmm.2019.166172

[27] Litewka, J. D., Łazarczyk, A., Hałubiec, P., Szafrański, O., Karnas, K., Karewicz, A., 2019. Superparamagnetic Iron Oxide nanoparticles—current and prospective medical applications. *Materials*, 12, pp. 617. doi: 10.3390/ma12040617

[28] Khan, D., Rahman, A.U., Kumam, P., Watthayu, W., Sitthithakerngkiet, K., Gala, A.M., 2022. Thermal analysis of different shape nanoparticles on hyperthermia therapy on breast cancer in a porous medium: A fractional model. *Heliyon*, 8, pp. 10170.

[29] Khan, D., Rahman, A.U., Kumam, P., Watthayu, W., 2022. A fractional analysis of hyperthermia therapy on breast cancer in a porous medium along with radiative microwave heating. *Fractal and Fractional*, 6, pp. 82. doi: 10.3390/fractalfract6020082

[30] Shokri, A. J., Tavakoli, M. H., Sabouri Dodaran A. A., Akhoundi Khezrabad, M. S., 2016. Numerical study of the influence of coil step on the induction heating process in three-dimensional. *Journal of Applied Electromagnetics*, 4, pp. 37-44.

[31] Rosensweig, R.E., 2002. Heating magnetic fluid with alternating magnetic field. *Journal of Magnetism and Magnetic Materials*, 252, pp. 370–374. doi: 10.1016/S0304-8853(02)00706-0

[32] Pennes, H.H., 1948. Analysis of tissue and arterial blood temperatures in the resting human forearm. *Journal of Applied Physiology*, 1(2), pp. 93-122. doi: 10.1152/jappl.1948.1.2.93

[33] Giustini, A.J., Ivkov, R., Hoopes, P.J., 2010. Magnetic nanoparticle hyperthermia in cancer treatment. *Nano Life*, 1(1), pp. 17-32.

[34] Dürr, S., Janko, C., Lyer, S., Tripal, P., Schwarz, M., Zaloga, J., Tietze, R., Alexiou, C., 2013. Magnetic nanoparticles for cancer therapy. *Nanotechnology Reviews*, 2, pp. 395–409.

[35] http://itis.swiss/virtualpopulation/tissue-properties/database/

[36] Rezaeian, M., Sedaghatkish, A., Soltani, M., 2019. Numerical modeling of high-intensity focused ultrasound-mediated intraperitoneal delivery of thermosensitive liposomal doxorubicin for cancer chemotherapy. *Drug Delivery*, 26, pp. 898–917. doi: 10.1080/10717544.2019.1660435

[37] Leeuwen, R.V., 2021. Development of an accurate temperature model for intraperitoneal hyperthermia. Master's Thesis, University of Twente.

[38] Liu, K., Wang, C., Cheng, P.J., 2013. Nonlinear behavior of thermal lagging in laser-irradiated layered tissue. *Advances in Mechanical Engineering*, 5, pp. 732575. doi: 10.1155/2013/732575

[39] Tang, Y., Jin, T., Flesch, R.C.C., Gao, Y., 2020. Improvement of solenoid magnetic field and its influence on therapeutic effect during magnetic hyperthermia. *Journal of Physics D: Applied Physics*, 53, pp. 235401. doi: 10.1088/1361-6463/ab87c5

[40] Rudnev, V., Loveless, D., Cook, R.L., 2017. Handbook of Induction Heating. 2nd ed. CRC Press, Boca Raton.

[41] Schooneveldt, G., Leijsen, Y.V., Balidemaj, E., Crezee, H., 2018. Clinical validation of a novel thermophysical bladder model designed to improve the accuracy of hyperthermia treatment planning in the pelvic region. *International Journal of Hyperthermia*, 35, pp. 383-397. doi: 10.1080/02656736.2018.1506164